Supplementary Information

The impact of dendrites and related compositional fluctuations on hydrogen absorption thermodynamics in *bcc* multi-principal element alloys

Veronica Enblom[1], Fernando Maccari[2], Franziska Sheibel[2], Aaron Keith[3,4], Vitalie Stavila[5], Claudia Zlotea[3], Oliver Gutfleisch[2], Paul F. Henry[1,6], Martin Sahlberg[1,*]

[1] *Department of Chemistry – Ångström Laboratory, Uppsala University, Box 538, 751 21 Uppsala, Sweden.*
[2] *Functional Materials, Institute of Material Science, Technical University of Darmstadt, 64287 Darmstadt, Germany.*
[3] *Université Paris-Est Créteil, CNRS, ICMPE, UMR 7182, 2 rue Henri Dunant, Thiais 94320, France*
[4] *School of Engineering and Materials Science, Queen Mary University of London, Mile End Campus, London E1 4NS, United Kingdom*
[5] *Sandia National Laboratories, Livermore, California 94551, USA.*
[6] *ISIS Pulsed Neutron & Muon Facility, Rutherford Appleton Laboratory, Harwell Campus, Didcot OX11 0QX, United Kingdom*

Keywords: Medium-entropy alloys, High-entropy alloys, Multicomponent alloys, Compositionally complex alloys, Hydrogen absorption, Hydrogen storage, PCT isotherms, Microstructure design.

* Corresponding author Email: martin.sahlberg@kemi.uu.se

Sample synthesis

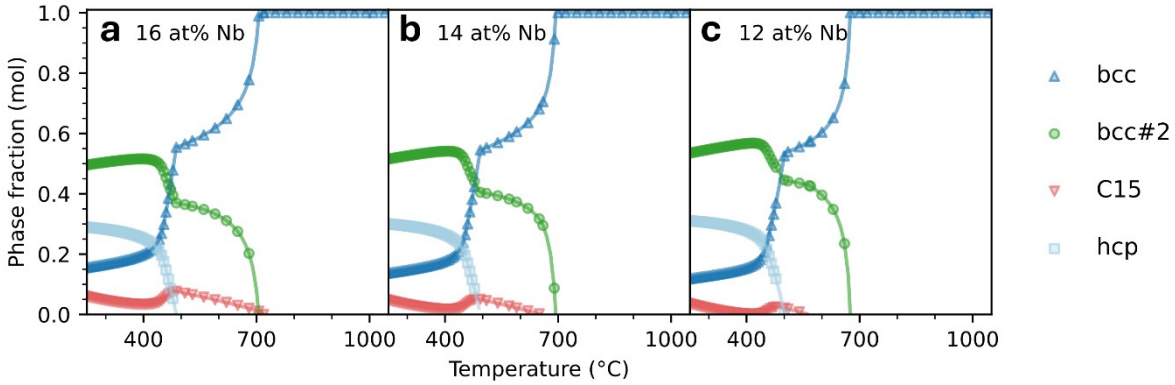

Figure S1: CALPHAD predicted phase fractions as a function of temperature for off-equimolar compositions in the TiVCrNb system of the form $Ti_{30+x}V_{30+x}Cr_{24}Nb_{16-2x}$, with x = 0 (a), 1 (b), and 2 (c). Decreasing the Nb-content suppresses the Laves phase, which shares a similar stability range with the secondary bcc phase at 16 at.% Nb.

Table S1: Unit cell parameters of the bcc phase derived from Pawley refinement of in-house XRD data for $Ti_{30}V_{30}Cr_{24}Nb_{16}$ alloys produced by arc melting, suction casting, melt spinning, and for suction-cast alloys annealed at 1000 °C for 14 days and 1400 °C for 1 h.

Sample	***a* (Å)**	**R_{wp}**	**χ^2**
Arc-melted	3.12167(2)	11.02	10.87
Suction cast	3.11833(3)	10.38	5.345
Melt spun	3.11456(11)	10.62	8.856
1000 °C, 14 days	3.14226(3)	10.27	17.67
1400 °C, 1 h	3.14013(100)	8.41	2.737

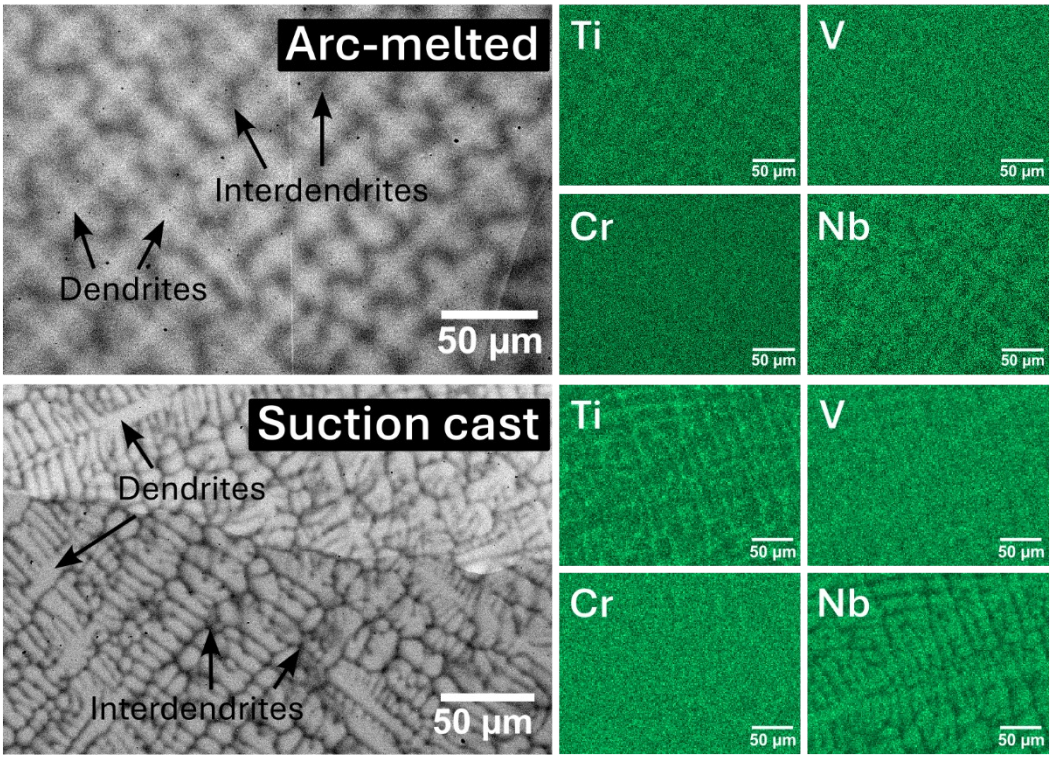

Figure S2: EDS elemental maps of $Ti_{30}V_{30}Cr_{24}Nb_{16}$ alloys produced by arc-melting (top row) and suction casting (bottom row), with corresponding SEM-BSE images on the left. SEM and EDS data were acquired from nearby regions of the same samples, as measurements were conducted at different times. Both alloys exhibit elemental partitioning, with Nb/V enrichment in dendritic regions and Ti/Cr enrichment in interdendritic regions. The suction-cast sample shows a finer microstructure and reduced segregation length scale relative to the arc-melted sample.

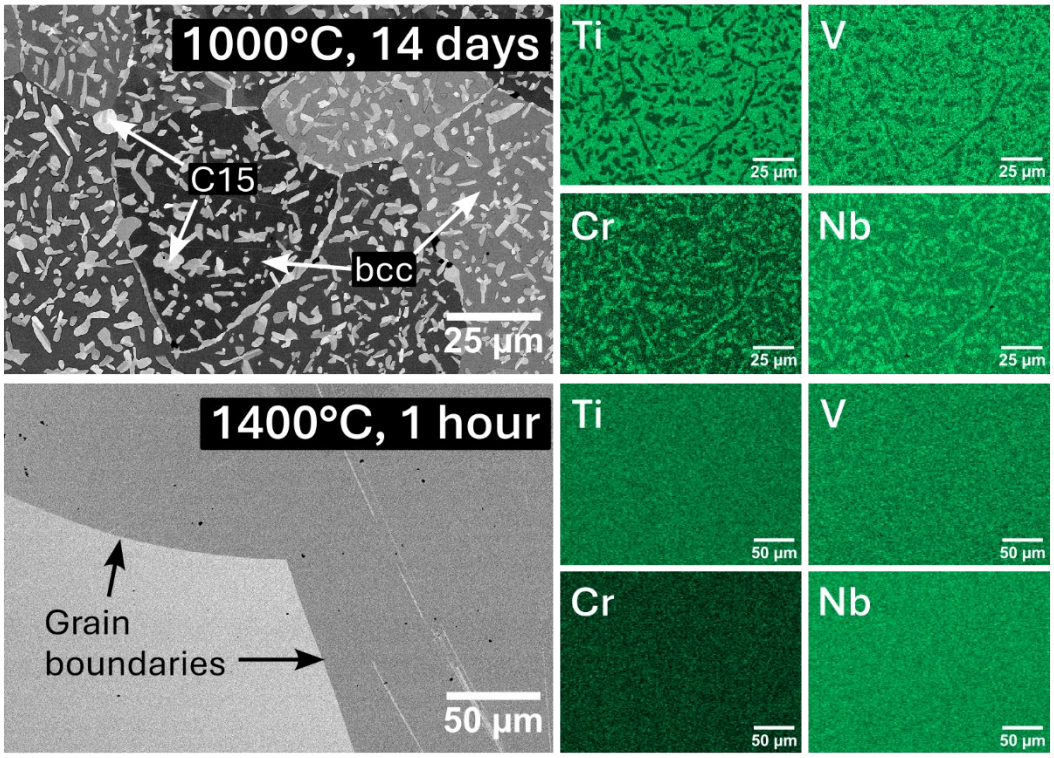

Figure S3: EDS elemental maps of suction-cast $Ti_{30}V_{30}Cr_{24}Nb_{16}$ alloys annealed at 1000 °C (top row) and 1400 °C (bottom row), with corresponding SEM-BSE images on the left. At 1000 °C, Nb- and Cr-rich precipitates are visible within and between grains, consistent with the formation of a secondary C15 Laves phase. The 1400 °C sample exhibits uniform elemental distributions, indicating a chemically homogeneous single-phase bcc structure.

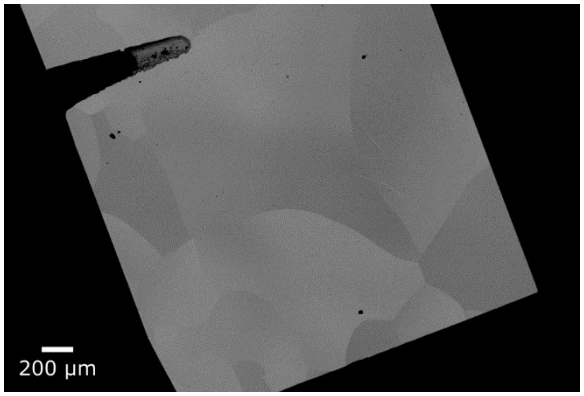

Figure S4: SEM-BSE image of a suction cast $Ti_{30}V_{30}Cr_{24}Nb_{16}$ alloy annealed at 1400 °C for 1 h. The microstructure is dominated by large, featureless grains, with no visible secondary phases or dendritic segregation.

Hydrogen absorption and thermodynamics

Figure S5 shows the first absorption curve for each sample, revealing the maximum capacity of each alloy and the approximate initial absorption rate. The homogenised sample exhibits a single absorption step, whereas the dendritic sample displays a three-step absorption profile. However, this behaviour cannot be attributed to differences in the reaction mechanism, as it reflects variations in the absorption onset between individual alloy pieces. Each sample was divided into three metal pieces to fit the reactor. Because these measurements were performed during the first absorption, before the metal pieces had pulverised, the pieces had different contact areas with the gas, leading to variations in absorption onset and rate. Consequently, no definitive conclusions can be drawn regarding differences in reaction mechanism or intrinsic absorption rate; only the maximum capacity can be reliably compared.

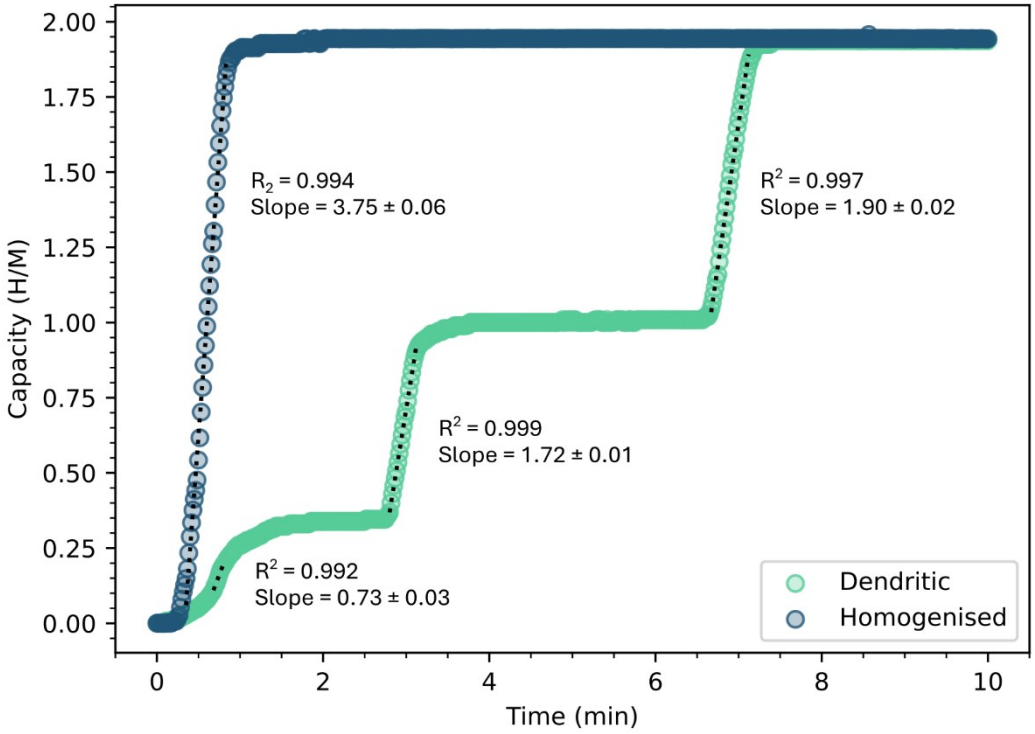

Figure S5: First hydrogen absorption kinetics of suction-cast $Ti_{30}V_{30}Cr_{24}Nb_{16}$ alloys at 25 °C and ≈54 bar H_2, measured after activation at 410 °C under dynamic vacuum for 3 h. The homogenised alloy (annealed at 1400 °C for 1 h) exhibits rapid, single-step absorption, reaching full capacity within two minutes. The dendritic (as-cast) alloy exhibits a three-step absorption profile, attributed to variations in onset among the three pieces used in the measurement. Dotted lines indicate linear fits used to estimate absorption rates, with uncertainties given as the standard error of the fitted slope.

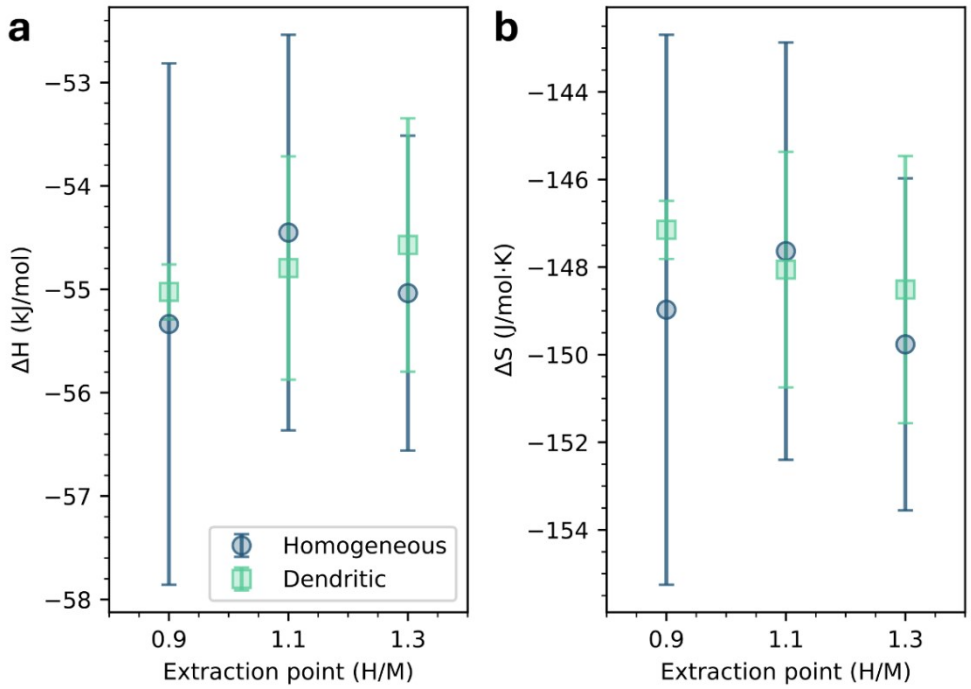

Figure S6: Hydride formation enthalpy (ΔH) and entropy (ΔS) for the monohydride-dihydride transition in suction-cast $Ti_{30}V_{30}Cr_{24}Nb_{16}$ alloys, derived from van't Hoff analyses using equilibrium pressures at H/M = 0.9, 1.1, and 1.3 along the plateau region. Squares and circles denote mean values from the van't Hoff fits for the alloy in the as-cast dendritic and homogenised (annealed at 1400 °C for 1 h) states, respectively, with error bars representing the standard deviation of the fit.

The lack of absorption in the melt-spun sample

Table S2: Unit cell parameters and phase fractions derived from Rietveld refinement of neutron diffraction data for $Ti_{30}V_{30}Cr_{24}Nb_{16}$ alloys produced by suction casting (homogenised at 1400 °C for 1 h) and melt spinning.

Sample	*a* (Å)	Oxide fraction (wt.%)	R_{wp}
Suction cast - 1400 °C, 1 h	3.117(6)	-	1.14
Melt spun	3.113(5)	<2	1.16

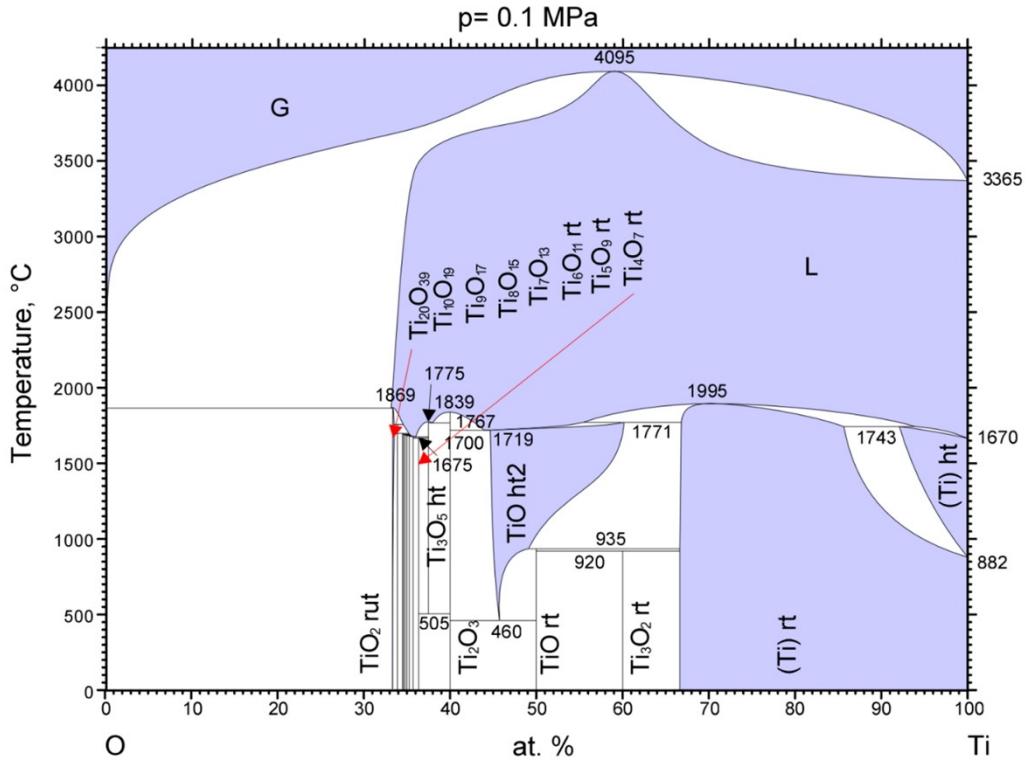

Figure S7: Ti-O binary phase diagram obtained from ASM International, Diagram No. 104180.